Collapse of Flexible−Semiflexible Copolymers in Selective Solvents: Single Chain Rods, Cages, and Networks

I. R. Cooke and D. R. M. Williams*

Research School of Physical Sciences and Engineering, Australian National University, Canberra 0200, Australia

Received October 13, 2003; Revised Manuscript Received April 21, 2004

ABSTRACT: We examine the single chain behavior of block copolymers with flexible and semiflexible blocks. For these flexible−semiflexible copolymers two different solvent conditions are examined. In one case the solvent is poor for the semiflexible blocks and good for the flexible blocks, and in the other this situation is reversed. When the solvent is poor for the semiflexible blocks, we find a rodlike state at high stiffness and an isotropic globule at low stiffness. For the opposing case where the solvent is good for the semiflexible blocks we observed the formation of single molecule networks. In these networks the collapsed flexible blocks form nodes linked together by semiflexible blocks. Such a system is in principle similar to a multichain associating telechelic, except that the linkers in this case are not flexible and are joined into a single chain. The number of nodes in these networks was found to vary linearly with the number of segments in the copolymer. For polymers with a relatively small number of segments, open tetrahedral cages were observed while those with many more segments formed larger networks comprised of many such tetrahedra.

I. Introduction

Under poor solvent conditions single polymer chains form a compact state that minimizes interfacial and bending energies. Even for simple homopolymers, a rich variety of compact states can occur, depending on chain stiffness and solvent quality. In the simple case of a fully flexible homopolymer this collapsed state is a spherical globule. However, as the chain stiffness is increased, toroids,[1,2] rods with hairpin bends,[3,4] and other structures such as disks[5] are known to form. The process of collapse for these semiflexible polymers and the characterization of their collapsed states has been a topic of much recent interest.[2,5−8] So far, however, all efforts in this area have focused on homopolymers, and very little is known about the collapse of polymers with variable stiffness along the chain. An obvious starting point in the study of polymers with variable stiffness is to take the simple case of a copolymer with alternating semiflexible and fully flexible blocks. In the case where the semiflexible blocks are very stiff, such polymers are referred to as rod−coil. Rod−coil copolymers are already well characterized in the melt, where they form nematic and smectic liquid crystal phases. More recently, however, there has been interest in nanoscale structures formed by aggregates of rod−coil copolymers in semidilute solution. Examples of such aggregates include tubes, mushrooms, stacked plates, and "hockey puck" geometries.[9−12] In this paper we also consider well-defined nanoscale geometrical structures; however, they are not formed from multichain aggregates. Instead, we consider long chains with sufficient numbers of flexible and semiflexible blocks as to allow the formation of aggregates within a single molecule. Our study is not restricted to the rod−coil case, and we consider a range of stiffness values for the semiflexible sections as well as two different selective solvent conditions. In particular, we will study the case where the solvent is poor for one of the monomer types (either semiflexible or flexible) and good for the other. Such solvent selectivity combined with differing stiffness results in some very interesting single molecule structures. We demonstrate the existence of a single molecule ordered rodlike state that has high nematic order, and we show that the isotropic−nematic transition for such a chain is sharp. We also predict the existence of single chain glassy networks for the opposing set of stiffness and solubility parameters.

II. Simulation Details

We used a coarse-grained model consisting of beads and springs to represent our polymer chains. Flexible−semiflexible type polymers were constructed from N beads divided into m blocks of equal length. Blocks were of alternating monomer types. For one type the solvent was poor, hereafter referred to as P, and for the other type the solvent was good, hereafter referred to as G. Except where otherwise mentioned, we studied chains with $N = 200$ and $m = 10$. To simulate the effect of solvent, we used two body interaction potentials between beads. For the P−P type interactions we used a standard Lennard-Jones potential

$$\frac{U_\alpha}{k_B T} = 4\epsilon\left(\left(\frac{\sigma}{r}\right)^{12} - \left(\frac{\sigma}{r}\right)^{6}\right) \qquad (1)$$

with $\epsilon = 1.2$ and $\sigma = 2.0$. Where the value of ϵ dictates the depth of the attractive minimum, σ can be thought of as an effective excluded-volume diameter for the beads and r is the interbead distance. Our choice of ϵ in this case was made simply on the basis that it be sufficient to induce collapse of individual blocks (for which $N = 20$) within our copolymer. A homopolymer with $N = 20$ exhibits a broad collapse transition that begins at $\epsilon \sim 0.5$ and is complete at $\epsilon \sim 1.1$ (using all other simulation parameters as in our system). We therefore chose $\epsilon = 1.2$ so as to obtain individual blocks that were fully collapsed. We were also careful to avoid using an excessively large value of ϵ which would result in highly ordered, solid collapsed globules rather than fluid ones. Nevertheless, we have conducted a small number of simulations with larger ϵ (e.g., 1.5, 2.0) for

10.1021/ma0355406 CCC: $27.50
Published on Web 06/24/2004

which the characteristic "dogbone" and "network" structures that we present in the following sections were also observed.

P−G and G−G type interactions were modeled as a purely repulsive potential

$$\frac{U_\beta}{k_B T} = \epsilon\left(\frac{\sigma}{r}\right)^{12} \tag{2}$$

with ϵ and σ taking the same values as in the P−P case. U_α and U_β potentials were truncated to 0 at 2.5σ.

Bonds between neighboring beads along the chain were modeled using an inverse Langevin type potential of the form

$$\frac{U_{\text{bond}}}{k_B T} = (\sigma)^{-1} l^*(r/(\sigma)) \tag{3}$$

This is equivalent to a Hookean type spring potential at short extensions but increases rapidly for extensions close to or beyond the bond length, σ. For practical purposes, we calculated U_{bond} using a Taylor series expansion in r to terms of order r.[20] This gives a close approximation to U_{bond} over the range of r in our simulation.

For the semiflexible blocks in our rod−coil copolymers we imposed a bending energy, U_{bend}, on one of the bead types (P or G) with the other type remaining fully flexible. U_{bend} is given by

$$\frac{U_{\text{bend}}}{k_B T} = -\kappa \cos\theta \tag{4}$$

where κ represents the stiffness of the chain segment and θ is the angle formed between two adjacent bead−bead bonds. In analytic work the continuum bending potential $U^l_{\text{bend}}/k_B T = \kappa'/2\int ds\ (d\theta/ds)^2$ is often used, where s is the arc length, θ is the tangent angle, and the integral is taken over an arc length of chain l. Our bending potential is essentially a discrete version of this common analytic model. Assuming a constant bond length a, the discrete and continuum models are related via the simple relationship $\kappa = \kappa'/a$. In the discrete model implemented in our computations we do not assume a constant a; however, this leads to rather cumbersome equations which we do not present here.

We studied polymers where one segment type (P or G) was fully flexible ($\kappa = 0$) and the other had some bending rigidity ($\kappa > 0$). Thus, our polymers could be broadly classified into two classes depending on which monomer type made up the semiflexible segments. These classes are referred to as "semiflexible P" or "semiflexible G" according to which monomers have $\kappa > 0$. Within these classes we explored a range of κ. At the junction between two bead types we assumed that the bending energy was always 0.

Bead motion was calculated by integrating the Langevin equation. Referring to dimensionless quantities throughout, we used a time step $\Delta t = 0.002$, diffusion constant $D = 1$, and thermal energy $k_B T = 1$. Brownian fluctuations caused by the motion of solvent particles are accounted for through the term $\eta(t)\sqrt{D}$, where $\eta(t)$ is a stochastic variable that is given by a Gaussian distribution with mean 0 and variance $2\Delta t$.

Since our simulation technique is stochastic in nature, we made replicate runs for each value of a parameter under investigation (usually κ). With a few exceptions which we discuss later, the following format was used for each run. A starting configuration was generated as a random walk and equilibrated for 1×10^6 time steps. During the equilibration phase the attractive P−P attraction was replaced by a pure repulsion similar to U_β. In other words, we equilibrate in good solvent conditions. After this initial equilibration, κ was set to its desired value, and the polymer equilibrated for a further 1×10^6 time steps. The system was then effectively quenched via the imposition of U_α for the P−P interactions, and the simulation was run to completion (a further 5×10^7 time steps).

III. Selective Solvents I: Semiflexible P, Flexible G

Semiflexible P type polymers exhibit two basic collapsed morphologies depending on the value of κ. On the basis of the snapshots shown in Figure 1, we see that for low stiffness the collapse process leads to an isotropic globule of P surrounded by a corona, consisting of loops of G. For high stiffness an ordered state is formed that resembles a rigid rod of P with end caps of G. In some cases the final structure formed for high stiffness is a perfect "dogbone" (see stage D for $\kappa = 10$ in Figure 1), whereas in other cases there are defects present (see stage C for $\kappa = 10$ in Figure 1). These defects generally appear in the form of a frustrated state where one of the G type blocks bridges between the two ends of the rigid rod of P. Such states result in an increase in both solvent and bending energies and are therefore clearly metastable (since entropic effects can be neglected in our poor solvent system). In the discussion below we present results where such defect states are removed (pruned data) as well as the full data where they are included. We used exactly three replicates to obtain pruned averages and five replicates for unpruned data.

To explore the transition between the isotropic and nematic collapsed morphologies, we calculated the liquid crystal order parameter, S, for the P type beads. To calculate S, it is first necessary to define a director $\hat{n}$. We simply define $\hat{n}$ as a unit vector with direction determined by the mean of all P−P bond vectors in the polymer, i.e.

$$\hat{n} = \left\langle \frac{\hat{r}_P}{|\hat{r}_P|} \right\rangle \tag{5}$$

where $\hat{r}_P$ is an P−P bond vector and $\langle ... \rangle$ represents the average over all such P−P bond vectors. S is now defined in terms of $\hat{n}$ as

$$S = \left\langle \frac{3}{2}(\hat{n}\cdot\hat{r}_P)^2 - \frac{1}{2} \right\rangle \tag{6}$$

In Figure 2 we present collapsed state averages of S for polymers with various stiffness values. Note that both pruned and unpruned data show a sudden increase in S as the stiffness is increased beyond $\kappa = 7$, but for the pruned data the increase is more uniform. This sudden transition from isotropic globule to highly ordered rod occurs in our poor solvent system where entropic effects are relatively minor. Thus, the transition is likely to be driven by the balance of bending and surface free energies. Although we cannot directly calculate the surface free energy in our solvent-free simulation model, we note that surface effects arise due

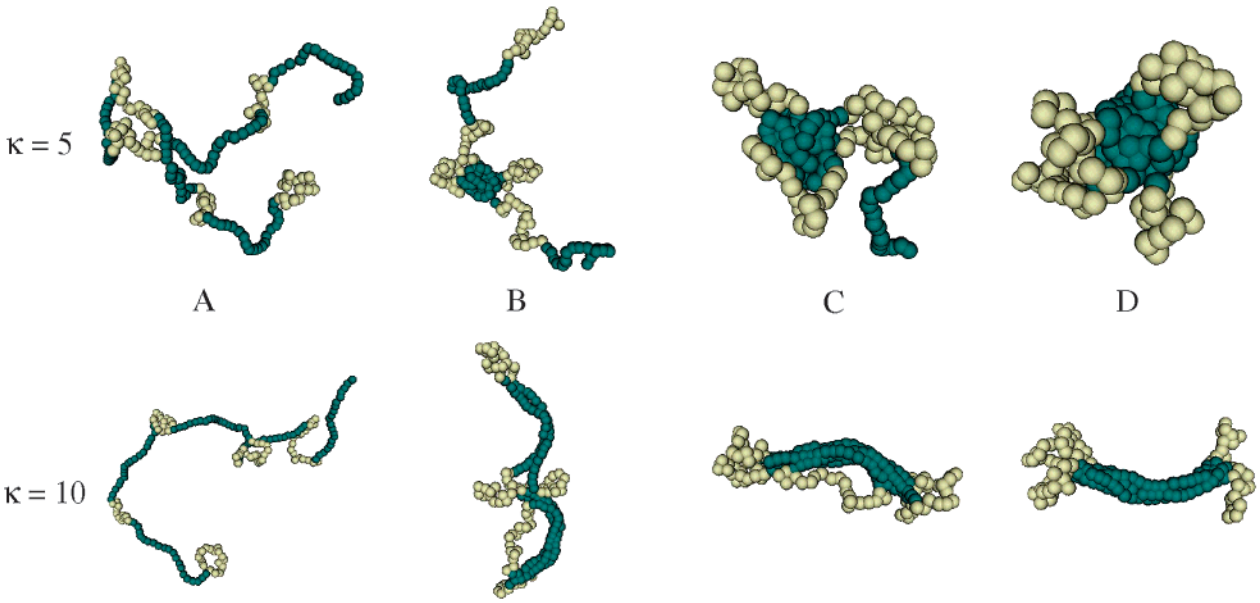

Figure 1. Typical folding sequence for semiflexible P type polymers with two different stiffness values, $\kappa = 5$ (top) and $\kappa = 10$ (bottom). Letters A−D represent successive stages in the collapse process. The precise simulation times corresponding to these stages varied strongly between simulation runs; however, as a general guide we give simulation times for the snapshots in this figure in alphabetical order as follows: for $\kappa = 5$, $t = 0$, 1, 5, 25; for $\kappa = 10$, $t = 0$, 5, 60, 200, where t is in units of 2.5×10^5 time steps.

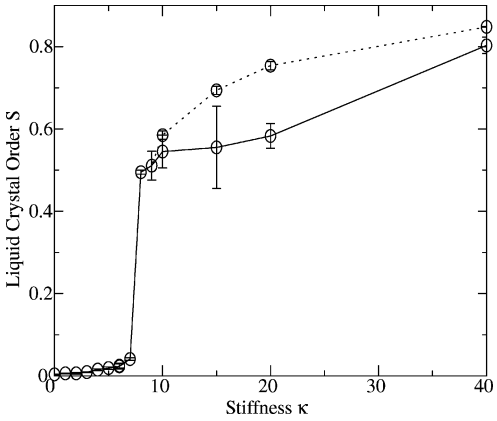

Figure 2. Average values of S vs stiffness for semiflexible P polymers. The dashed line represents pruned values, and the solid line represents full data. Averages are over five replicate runs (three for pruned data), and error bars show the standard error in these samples. Values of S for each replicate were obtained from time averages over the last 1×10^7 time steps of the simulation.

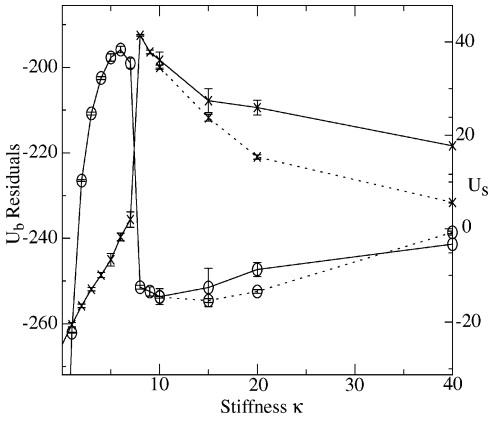

Figure 3. Average values of the bending energy U_{bend} (circles) and the solvent energy U_s (crosses) vs stiffness for semiflexible P polymers. The dashed line represents pruned values, and the solid line represents full data. Averages are over five replicate runs (three for pruned data), and error bars show the standard error in these samples. Values of S for each replicate were obtained from time averages over the last 1×10^7 time steps of the simulation.

to nonbonded potentials in our system and calculate the sum of these potentials instead, $U_s = U_\beta + U_\alpha$. We call this the solvent energy. In Figure 3 we explore these two contributions (U_{bend} and U_s) to the total internal energy of the polymer as a function of stiffness. In constructing this plot, we have taken account of the fact that the bending energy varies systematically and linearly with the stiffness. Our aim was to examine only changes in U_{bend} superimposed on this systematic variation. To achieve this, we have plotted the residuals $U_{\text{bend}}^{\text{res}} = U_{\text{bend}} - U_{\text{bend}}^{\text{fit}}$ vs κ, where $U_{\text{bend}}^{\text{fit}}$ is obtained from a linear regression of U_{bend} vs κ. By plotting $U_{\text{bend}}^{\text{res}}$, we see how U_{bend} deviates from a simple linear relationship. In particular, we see a dramatic decrease in the bending energy as the polymer transforms from globule to the ordered rod. This decrease in bending energy is compensated for by a simultaneous increase in surface energy, which reflects the increased surface area of the rod compared with the globule.

It is interesting to compare the isotropic to nematic transition seen here with the well-known transition from globule to torus in a semiflexible homopolymer. In that case there is already some evidence that the transition is first order in nature.[13] The transition presented here is quite similar, except that instead of a continuous homopolymer we have a collection of polymer segments. Because these segments can straighten individually, they are able to form a stable rod, whereas the homopolymer must form a torus to obtain uniform bending. In both cases the transition is driven by a competition between solvent energy, which is higher in the rod and torus than in the globule and bending energy which is highest for the globule at a given stiffness.

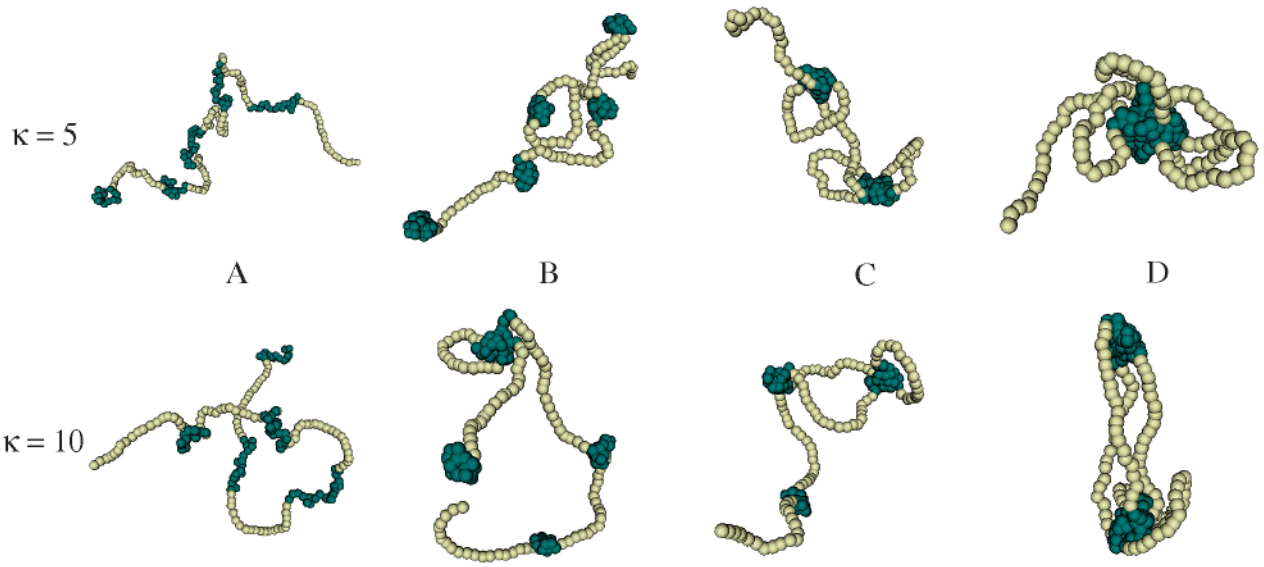

Figure 4. Typical folding sequence for semiflexible G type polymers with two different stiffness values $\kappa = 5$ (top) and $\kappa = 10$ (bottom). Letters A−D represent successive stages in the collapse process. The precise simulation times corresponding to these stages varied strongly between simulation runs; however, as a general guide we give simulation times for the snapshots in this figure in alphabetical order as follows: for $\kappa = 5$, $t = 0$, 2, 15, 100; for $\kappa = 10$, $t = 0$, 5, 60, 150, where t is in units of 2.5×10^5 time steps.

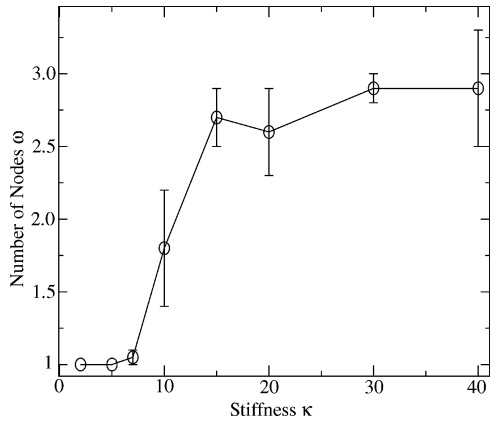

Figure 5. Average number of clusters for collapsed semiflexible G type polymers as a function of stiffness. Averages are over five replicate runs. The value for each replicate is obtained as a time average over the final 1×10^7 time steps of the simulation.

IV. Selective Solvents II: Flexible P, Semiflexible G

In Figure 4 we present typical snapshots of the collapse process for semiflexible G type polymers. As with the semiflexible P case, we again observed two distinct behaviors depending on the value of stiffness. For relatively small values of κ, the poor solvent P type beads are able to coalesce and form a single globule, with the semiflexible G segments forming loops around this globule. Since the single globule state involves considerable bending of G type blocks, it becomes less favorable as κ is increased. In Figure 5 (stage D for $\kappa = 10$) we see that beyond a certain critical κ the number of P type clusters in the collapsed state becomes more than 1. By forming such a multiple cluster state, the system is able to eliminate the requirement that the G segments undergo bending; however, this free energy gain is offset by the penalty involved in breaking the P type globule into smaller globules. We can make a rough calculation of the transition point between single and multiple globules based on a free energy argument that neglects entropic effects. Such an assumption is not as drastic as it may at first seem since in our system the poor solvent ensures that all P type monomers are confined to tight clusters, and the stiffness of the G type monomers confines them to relatively well-ordered, rodlike states.

The free energy of a single globule state, F^1, is given by the sum of the globule free energy F_g^1 and the bending free energy F_b^1. The globule free energy can be estimated by assuming an effective surface tension γ such that $F_g^1 = \gamma 4\pi R_g^2$, where R_g is the globule radius. R_g can be calculated from the fact that for a single collapsed globule the volume is simply the sum of volumes of constituent beads, i.e., $R_g^3 = N(a/2)^3$, where $a/2$ is the bead radius. To calculate the bending free energy F_b^1, we assume that the G type blocks are long compared with R_g. Under this assumption the shape that minimizes bending energy is simply a circle that starts and ends at the globule. The bending free energy of a single circular G type section of length l is

$$f_b = \kappa'/2 \int_0^l \mathrm{d}s\, 4\pi^2/l^2 = 2a\kappa\pi^2/l \qquad (7)$$

Thus, a chain with m blocks has total bending energy $F_b = m2a\kappa\pi^2/l$. To find the critical value of κ for which the single globule state becomes unstable, we compare its free energy, F^1, with that of a two globule network, F^2. Since the G type monomers in the two globule state are able to bridge between globules, they do not need to bend, and therefore $F_b = 0$. Since there are two globules, F_g^2 is given by the sum of their respective energies, i.e., $F_g^2 = 2\gamma\pi N^{2/3}a^2/2^{2/3}$. Comparing F^1 and F^2, we find that the critical stiffness κ_c is given by

$$\kappa_c = \frac{l\gamma a N^{2/3} C}{m} \qquad (8)$$

where C is a numerical constant with the value $1/\pi(1/2^{2/3} - 1/2) \sim 0.04$. We can now make a rough comparison of eq 8 with the location of the transition point in Figure 5. An approximate value for the surface tension can be

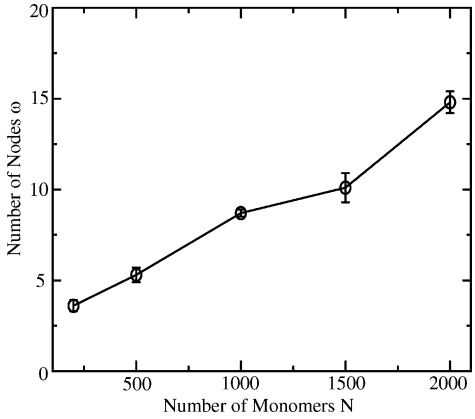

Figure 6. Number of nodes ω as a function of polymer length N for polymers with the same flexible−semiflexible block length. Error bars shown represent standard errors of a mean from three replicate simulation runs.

obtained via the following argument. We assume that the solvent energy of a bead is given by $-n\epsilon$, where n is the number of immediate neighbors. For a bead in the bulk of the globule we assume that $n = 6$ and at the surface $n = 3$. According to this approximation, a bead at the surface contributes $E \sim 3\epsilon$ to the energy, and since it occupies a surface area of $A \sim \pi a^2/4$, we have $\gamma \sim E/A \sim 12\epsilon/4\pi$. Within the context of the approximations made already we then have $\gamma \sim 1$. Substituting this and all other numerical constants into eq 8, we obtain $\kappa_c \sim 11$ (note that we used the relations $l = Na/m$ and $a \sim \sigma = 2$ to make this calculation). Given the approximate nature of our calculation, this compares favorably with the location of the transition point in Figure 5.

Equation 8 is only strictly valid for comparing single vs double cluster states. Although we are unable to generalize this result to the case where multiple clusters form, we were able to investigate such systems using computer simulation. Because of the relatively small size of the polymers studied so far ($N = 200$, $m = 10$), there has been little potential for multiple cluster formation. Nonetheless, it is clear that as the number of clusters increases, so too should the complexity of interconnecting G type monomers between them. Such a situation suggests that we might obtain a network with nodes of P and rigid linkers of G.

To explore states with large numbers of clusters and the potential for network formation, we examined a range of polymers with chain lengths in the range $N = 200$ to $N = 2000$. In each case we performed three replicate runs and used $m = N/20$ with a constant stiffness of $\kappa = 40$ for all the G type blocks. This ensures that the local structure of each chain remains the same irrespective of polymer length. To obtain good steady-state results for the largest polymers, it was necessary to run simulations for 1×10^8 time steps. As an indicator of the size of the network we calculated the number of nodes ω. We found that ω reached a steady state after at most 5×10^7 time steps, and we calculated the average of this value $\bar{\omega}$ over the final 2.5×10^7 time steps of the simulation for each of three replicates. In Figure 6 we see that a plot of average values of $\bar{\omega}$ vs N is approximately linear with very little spread of values about the fitted line. Such a linear relationship probably reflects the fact that regardless of size all the polymers studied have the same local structure in terms of the chain sequence. This uniformity of chain sequence

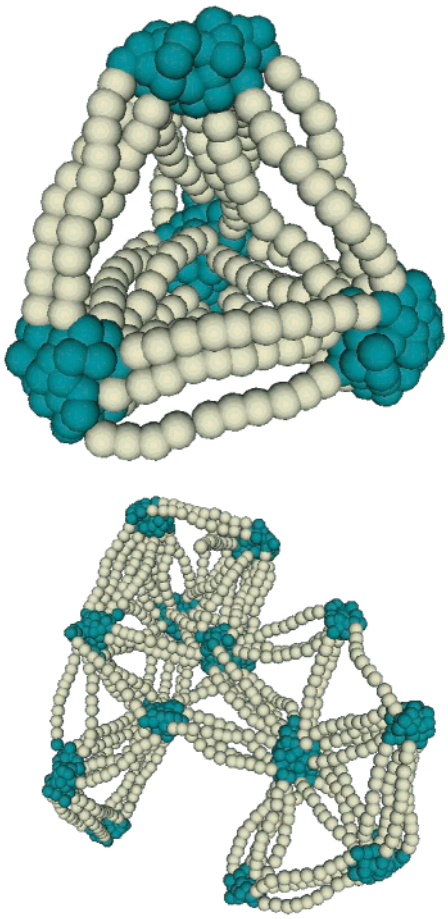

Figure 7. Collapsed steady-state semiflexible G type polymers with chain lengths $N = 500$ and $N = 2000$.

structure is in turn reflected in the uniformity of the three-dimensional structure of the network. We can see this in Figure 7, which shows the final steady-state structures for an $N = 500$ and an $N = 2000$ monomer chain. Both are comprised of nodes and links which form a triangular lattice. In the $N = 500$ polymer this consists of just one tetrahedral structure whereas in the $N = 2000$ polymer there are several such structures.

The structures shown in Figure 7 are steady-state structures in the sense that once formed they showed little change in ω over a period of $\sim 2.5 \times 10^7$ time steps. It is quite possible that these structures are metastable rather than globally stable, and the nature of the true minimum energy state is not clear. Even so, a brief look at the structures themselves suggests that these interconnected states should be extremely long-lived. In order for one node to coalesce with another, it would be necessary to simultaneously break apart and rearrange a large number of links. The activation barrier for such a process is of course extremely high, and we should probably regard the structures in Figure 7 as representing kinetically frozen or glassy states.

V. Conclusions

In this paper we have endeavored to map out some of the fundamental types of collapsed morphologies for flexible−semiflexible block copolymers. Although we have restricted ourselves to the simplest case of regular blocks with just two monomer types, we find a rich diversity of structures. In the semiflexible P case we found single chain rod structures that exhibit a sharp

isotropic to nematic transition as stiffness is increased. In the semiflexible G case we found that large systems form open and highly connected single molecule networks. Although our results on these glassy networks merely demonstrate the possibility of their existence, we would expect that they should not be too difficult to construct experimentally. Since the openness of the network and its size can easily be controlled, we can envisage a large number of potential applications including possible molecular "cages" for particles of various sizes. There is also the potential to create a macroscopic sample of these networks by allowing individual molecules to form collapsed multichain aggregates. Multichain aggregates are commonly observed for associating polyelectrolytes such as telechelic polymers where they can form mesoscopic "flower" micelles[14,15] or gels.[16] We anticipate that our system should also be capable of forming gels or mesoscale aggregates and that such aggregates would have an extremely uniform and tunable hole size. The key aspect of our system which allows this is the presence of stiff intermediate segments between the flexible stickers. These stiff segments result in a triangular lattice with a hole size that can be altered by changing the segment length.

References and Notes

(1) Bloomfield, V. A. *Curr. Opin. Struct. Biol.* **1996**, *6*, 334−341.
(2) Yoshikawa, K.; Takahashi, M.; Vasilevskaya, V. V.; Khokhlov, A. R. *Phys. Rev. Lett.* **1996**, *76*, 3029−3032.
(3) Schnurr, B.; Gittes, F.; Mackintosh, F. C. *Phys. Rev. E* **2002**, *65*, 061904.
(4) Hu, D.; Yu, J.; Wong, K.; Bagchi, B.; Rossky, P. J.; Barbara, P. F. *Nature (London)* **2000**, *405*, 1030−1033.
(5) Ivanov, V. A.; Stukan, M. R.; Vasilevskaya, V. V.; Binder, K. *Macromol. Theory Simul.* **2000**, *9*, 488−499.
(6) Schnurr, B.; Mackintosh, F. C.; Williams, D. R. M. *Europhys. Lett.* **2000**, *51*, 279−285.
(7) Kuznetsov, Y. A.; Timoshenko, E. G.; Dawson, K. A. *J. Chem. Phys.* **1996**, *105*, 7116−7134.
(8) Noguchi, H.; Yoshikawa, K. *J. Chem. Phys.* **2000**, *113*, 854−862.
(9) Williams, D. R. M.; Fredrickson, G. H. *Macromolecules* **1992**, *25*, 3561−3568.
(10) Jenekhe, S. A.; Chen, L. X. *Science* **1998**, *279*, 1903−1906.
(11) Stupp, S. I.; LeBonheur, V.; Walker, K.; Li, L. S.; Huggins, K. E.; Keser, M.; Amstutz, A. *Science* **1997**, *276*, 384−389.
(12) Sayar, M.; Stupp, S. I. *Macromolecules* **2001**, *34*, 7135−7139.
(13) Stukan, M. R.; Ivanov, V. A.; Grosberg, A. Y.; Paul, W.; Binder, K. *J. Chem. Phys.* **2003**, *118*, 3392−3400.
(14) Semenov, A. N.; Joanny, J.-F.; Khokhlov, A. R. *Macromolecules* **1995**, *28*, 1066−1075.
(15) Timoshenko, E. G.; Kuznetsov, Y. A. *Europhys. Lett.* **2001**, *53*, 322−327.
(16) Tanaka, F. *J. Non-Cryst. Solids* **2002**, *307*, 688−697.

MA0355406